Complex beam profiles for laser annealing of thin-film CdTe photovoltaics

Nicholas Goffin, John Tyrer, and Elliot Woolley

Articles you may be interested in

Theoretical model for ablation of thick aluminum film on polyimide substrate by laser etching
Journal of Laser Applications **30**, 042002 (2018); 10.2351/1.5054591

Complex beam profiles for laser annealing of thin-film CdTe photovoltaics

Nicholas Goffin,[1,a)] John Tyrer,[2] and Elliot Woolley[1,b)]

[1]*Centre for Sustainable Manufacturing and Recycling Technologies (SMART), Wolfson School of Mechanical, Electrical and Manufacturing Engineering, Loughborough University, Leicestershire LE11 3TU, United Kingdom*
[2]*Optical Engineering Research Group, Wolfson School of Mechanical, Electrical and Manufacturing Engineering, Loughborough University, Leicestershire LE11 3TU, United Kingdom*

Within the family of thin-film photovoltaics (PV), cadmium telluride has the fastest growing market share due to its high efficiencies and low cost. However, as with other PV technologies, the energy required to manufacture the panels is excessive, encompassing high environmental impact and manufacturing energy payback times of the order of 2–3 years. As part of the manufacturing process, the panels are annealed at temperatures of approximately 400 °C for 30 min, which is inherently inefficient. Laser heating has previously been investigated as an alternative process for thin-film annealing, due to its advantages with regard to its ability to localize heat treatment, anneal selectively, and its short processing time. In this investigation, results focusing on improvements to the laser-based annealing process, designed to mitigate panel damage by excessive thermal gradients, are presented. Simulations of various laser beam profiles are created in COMSOL and used to demonstrate the benefit of laser beam shaping for thin-film annealing processes. An enabling technology for this, the holographic optical element, is then used to experimentally demonstrate the redistribution of laser beam energy into an optimal profile for annealing, eliminating thermal concentrations. © *2018 Laser Institute of America*. https://doi.org/10.2351/1.5038072

Key words: laser annealing, thin-film, CdTe, thermal simulation, photovoltaics

I. INTRODUCTION

In recent years, the use of solar photovoltaics (PV) has increased worldwide as part of efforts for a more sustainable electricity generation and decarbonization of the energy grid. In the UK, 2.4 GW of PV capacity has been installed as of the 4th quarter of 2013,[1] representing 3% of total electrical generation capacity.[2] This is expected to reach a total of 9.3–10.7 GW by the end of the decade. In the United States, the Solar Energies Industry Association (SEIA) report for 2014[3] showed that by the end of 2014, a total of 18.3 GW of solar PV was operating in the United States, with additional installations in 2014 accounting for 32% of new generating capacity brought online that year. The vast majority of the total solar PV installations have occurred since 2010, increasing year on year.[3]

This high level of growth brings the issue of "energy payback" into greater focus. This is the concept that the net energy produced by a solar panel is the difference between the gross energy output of the panel and the energy used to manufacture it. After a panel is placed in operation, it needs to "repay" the manufacturing energy before it can be considered to be producing net energy. This repayment takes a certain amount of time and the smaller this time is, the greater the benefit the panel provides.

Historically, the solar PV market has been dominated by bulk crystalline silicon devices.[4] However, from a material use point-of-view, these devices are expensive and inefficient. The current generation of thin-film devices has inherent advantages in their use of materials, by coating a low-cost substrate with a thin layer of absorber, as well as a greater suitability for mass-production. These thin-film technologies can be categorized according to their core materials into four main groups: cadmium telluride (CdTe), amorphous silicon (a-Si), copper indium gallium selenide, and gallium arsenide. The first three are the most commonly used for terrestrial applications, while the latter is generally restricted to spacecraft applications, where the need for high efficiency outweighs its high cost. Within the thin-film arena, CdTe technology has the lowest energy payback time and manufacturing emissions.[5,6]

Regarding a CdTe panel, reducing the energy payback time can be achieved in two possible ways: By improving the panel efficiency so the panel produces more energy in a shorter period or by reducing the energy used during its manufacture. In this paper, the second method is addressed, with an optical method for the annealing stage of CdTe panel manufacturing that shows promise in the reduction of energy payback time. A review of literature is conducted covering current research in the use of lasers for annealing of CdTe and concluding with a description of the capabilities and previous research on Holographic Optics.

In this work, simulation setup and simulation results are presented together, investigating the heat transfer characteristics

a)Present address: Manufacturing Technology Centre Limited, Ansty Park, Coventry, CV7 9JU, United Kingdom.
b)Author to whom correspondence should be addressed; electronic mail: e.b.woolley@lboro.ac.uk. Telephone: +44 (0)1509 225410.

of different laser beam thermal profiles. Experiments are then used to verify the ability of modified thermal profiles to alter heat flow in the panel, as well as to evaluate the accuracy of the thermal simulations in their predictions. These results are discussed and opportunities for further development are identified.

II. CADMIUM TELLURIDE IN PHOTOVOLTAICS

CdTe photovoltaics require activation by annealing in the presence of chlorine in the form of either $CdCl_2$ or $MgCl_2$[7] at 400–450 °C. Potter et al.[8] experimented with this at 400 °C, finding that the annealing process gave an improvement in cell efficiency, provided that the annealing time was no longer than 10 min. Experiments with $CdCl_2$ annealing at temperatures of 200, 400, and 450 °C in both air and nitrogen atmospheres were conducted by Spalatu et al.[9] $CdCl_2$ was found to promote recrystallization and improve efficiency, provided that the concentration of Cl was not too high. A common annealing method is to deposit $CdCl_2$ as a separate layer on the surface of the CdTe and then anneal the entire panel.[8,10]

A. Using lasers to anneal CdTe photovoltaics

Laser-material interaction is a well-researched and understood field for many applications. Problems in annealing of materials have been addressed for ceramics,[11] while methods for processing with various TEM modes have been presented.[12,13] A useful review of current laser annealing methods is provided in Ref. [14].

A method of annealing that has gained recent attention is the use of lasers as heat sources. This has certain advantages, such as localized heat treatment, very selective annealing, short process duration and precise control of the heating time, and ramp up rate.[15] Kim et al. used an 808 nm wavelength diode laser to anneal CdTe thin films.[16] They found that the optical properties of CdTe mean that an 808 nm wavelength is considered the optimal commercially available wavelength to use, since the photon energy needed to be high enough for the beam to interact with the CdTe (wavelength <825 nm), but not so high that the beam is fully absorbed by the local surface without penetrating. The use of this method gave recrystallization and grain growth in the CdTe with heating times in the region of 15 s. Longer wavelengths of irradiation are not ideal for energy efficient annealing since CdTe becomes highly transparent above 900 nm. Other recent work on laser annealing of CdTe has used laser sources of 1064 nm, using the proportion of the beam that is transmitted for in situ process monitoring.[17]

However, limitations exist in the laser process so far described. Lasers generate a very high thermal gradient which, since the glass substrate is brittle, easily causes fracture. In the research so far described, this is avoided by rapid scanning using a galvanometer to gently warm the substrate over several seconds using multiple passes. This technique does not possess a great deal of scalability, since the area that can be covered is limited to the size of the galvanometer head.

B. Holographic optical elements in laser materials processing

The purpose of this study is to investigate the use of custom laser beam heat profiles to control laser beam heat flow in CdTe annealing. Standard laser beams, while having the advantages described in Sec. II A, suffer from disadvantages regarding their thermal profiles. The irradiance profile of a laser beam directly affects the thermal cycle undergone by the material that is being processed.[18]

Standard laser beams are known as TEM_{00} beams, which have a circular spot and a Gaussian thermal distribution.

This beam shape means that when the beam is traversing, the area of the panel heated by the beam is processed for different lengths of time and with different levels of intensity, depending upon which region of the beam is interacting with it. This results in a non-uniform process that anneals some areas of the panel more effectively than others, due to the differences in their thermal cycles.

Certain technologies exist that can alter the beam in a limited fashion, usually into one of the three types of beams, as illustrated in Fig. 1. The first type [Fig. 1(a)] is known as a "top hat" beam, where the spot is circular but with a uniform intensity profile. The second type [Fig. 1(b)] is commonly known as a ring or "rolo" beam, where the spot is circular with the energy concentrated at the outer edge. These are commonly generated by use of axicon lenses.[19] Wellburn et al.[20] used rolo beams for laser hardening, showing that altering the relative intensities of the ring and the center gave different hardened properties to the material. Some diode lasers are capable of producing a uniform rectangular beam, known as a "pedestal" as shown in Fig. 1(c). This has been demonstrated on a number of occasions in laser metal cladding by Mok et al.,[21] Riveiro et al.,[22] among others.

Although these beam types are superior in performance to a standard TEM_{00} beam, they represent the maximal optimization that the majority of beam shaping techniques are
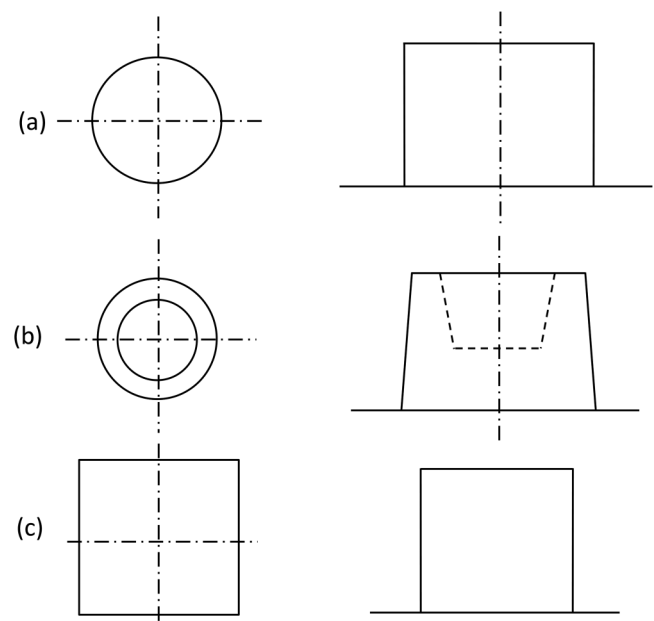
FIG. 1. Common laser beam profiles: (a) top hat, (b) rolo, and (c) pedestal.
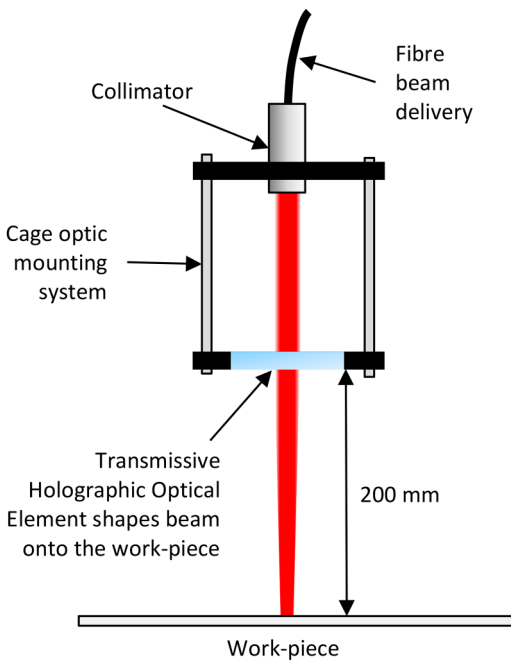
FIG. 2. Schematic of holographic beam delivery system.

capable of producing. In this work, it is asserted that in order for laser beam annealing to be fully effective, a greater level of control over the thermal profile is required.

A suitable technology for beam control is a device called a holographic optical element (HOE).[23] These use a computer generated kinoform to reshape an input laser beam into the desired thermal profile. A schematic of the optic itself, and the beam delivery system, is given in Fig. 2.

This means that the standard methodology of trying to achieve the best possible result with a given laser beam no longer applies; the desired result can be specified first and then a HOE created to give the required laser beam thermal profile. Previous HOE research has shown positive results in the areas of laser welding,[24,25] where complex asymmetrical beam profiles were used to create wide uniform weld tracks; powder-bed laser cladding,[26] where they were used to control fluid flow and grain growth; wire-based laser deposition,[27,28] to control dilution and increase energy efficiency; and initial work on laser annealing.[29]

The ability of holographic optics to control heat flow means that heat transfer simulations can then take on a powerful role in the optimization of experimental design. In simulation, the heat flux can be matched to the desired output and customized accordingly. HOEs allow a physical laser beam to be created that matches this customized heat flux. Simulated conditions can then be realized in practice and the process optimized.

In this work, laser beam heat transfer simulations are created and used to demonstrate the progressive optimization of a laser beam profile and the resultant effects on CdTe panel temperature distribution. These simulations are vital to process development, because they allow the rapid optimization of the laser beam profile without the time and expense of iteratively creating optics and testing them.
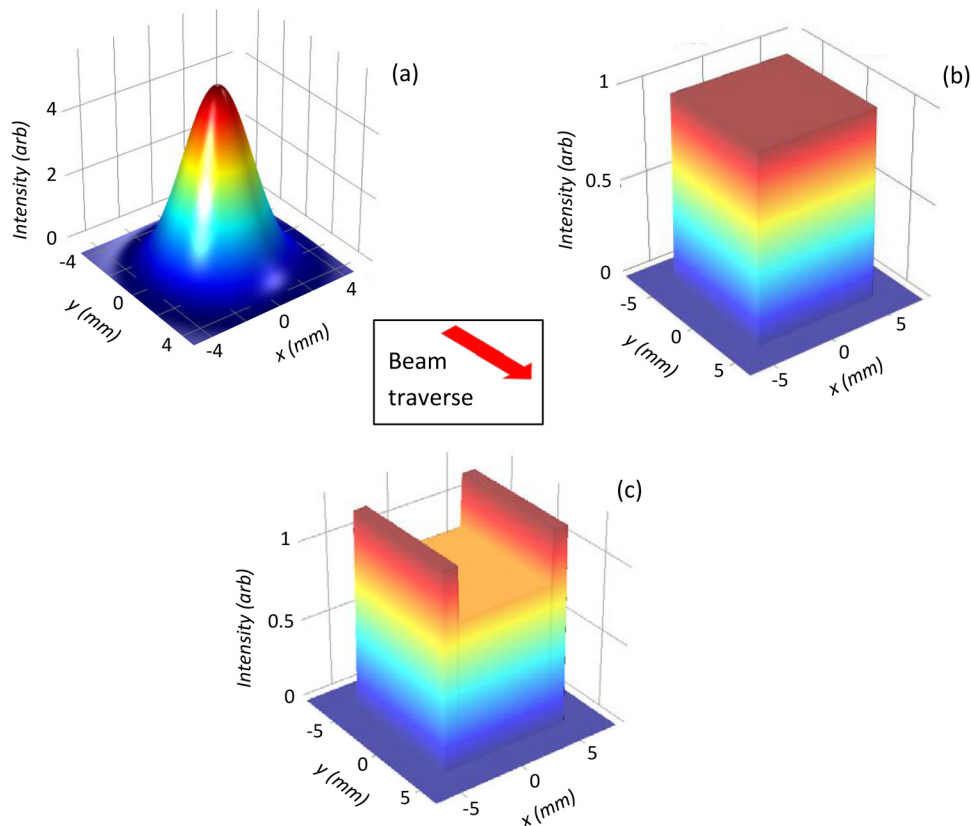
FIG. 3. Beam profile plots of (a) Gaussian, (b) pedestal, and (c) rugby posts beams.
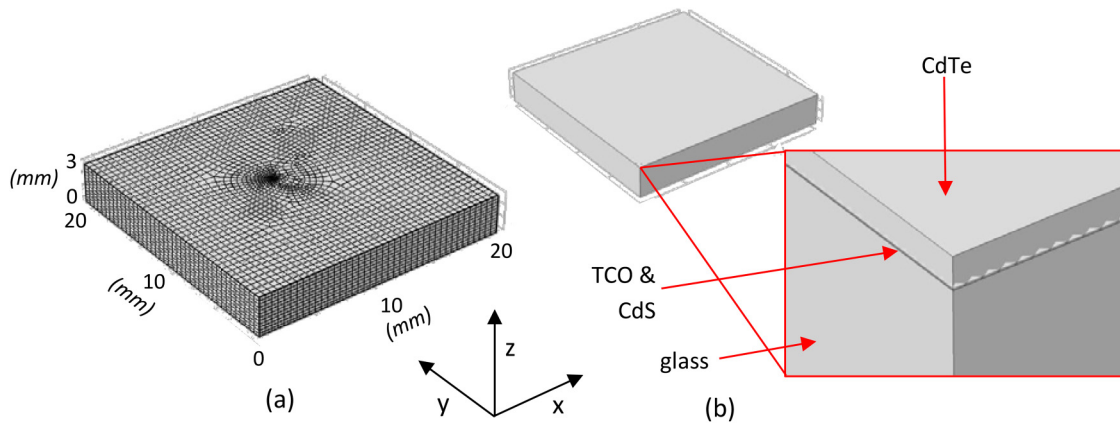
FIG. 4. Images showing (a) solar panel meshing and (b) the panel geometry with the relative thicknesses of the various layers. Panel dimensions are given in standard form using μm.

The second part of this work demonstrates the experimental use of a HOE and compares these results with those obtained from the simulations.

III. SIMULATION SETUP

COMSOL Multiphysics was used for the heat flow simulations, simulating three different beam profiles which are plotted in Fig. 3.

First, a 10 mm diameter TEM$_{00}$ Gaussian beam was plotted, in order to demonstrate the effects of the most commonly used beam type; this type is shown in Fig. 3(a). Second, a 10×10 mm pedestal beam was used, which is designed to mitigate the two main problems associated with Gaussian beams by altering the beam cross section from a circle to a square and replacing the Gaussian irradiance distribution with one that is uniform, as shown in Fig. 3(b).

Figure 3(c) shows a 10×10 mm "rugby posts" beam; so named for the thermal peaks at the outer edges. This profile was included to investigate the possibility of placing additional heat at the outer edges of the beam to counteract additional heat losses there. The peaks were each set at 1.25 mm width and $1.25 \times$ nominal irradiance. The central portion was reduced to $0.92 \times$ nominal irradiance to compensate and keep the overall irradiance equal to the pedestal beam from Fig. 3(b).

A. Mesh creation

In order to minimize computing time, a 20×20 mm panel was created. The model consisted of four layers:

- 3 mm thick substrate with soda lime glass material properties
- 50 nm thick transparent conducting oxide (TCO) layer with ZnO material properties
- 70 nm thick CdS layer
- 2 μm thick CdTe layer

The modeled panel geometry is shown in Fig. 4.

A swept mesh was used, with mesh size tied to beam size in the x and y axes, giving 20 elements across the beam width and a total of approximately 110 000 elements. The large number of elements was due to the z axis, where the enormous differences in the layer thicknesses, as shown in Fig. 4(b), meant that a biased mesh was used with twelve elements per layer.

Correlation of CdTe n and k values with wavelength shows very little change between wavelengths of 650–850 nm,[30] with

TABLE I. Parameters used for heat conduction model.

Parameter name	Parameter quantity	Parameter description
P_laser	10 (W)	Laser power
b_w	2.5 (mm)	Half of beam width
x0	w/2	Position of beam in x axis (mm)
b_l	2.5 (mm)	Half of beam length
l	20 (mm)	Panel length
w	20 (mm)	Panel width
glass_h	3 (mm)	Glass thickness
ZnO_h	50 (nm)	Zinc oxide layer thickness
CdS_h	70 (nm)	Cadmium sulfide layer thickness
CdTe_h	2 (μm)	Cadmium telluride layer thickness
P_d	P_laser/(4*(b_w)* (b_l))	Power density
r_beam	5 (mm)	Gaussian beam radius
CdTe_abs	0.76	CdTe 808 nm laser absorptivity
Period	30 (s)	Total simulation time

TABLE II. Beam position variables used in heat conduction simulations.

Variable name	Variable quantity	Variable description
trav	2 (mm/s)	Laser traverse velocity
ss	if(t<=0,0,t-0)	Time based modifier for beam position, here incorporating a 0 s start delay in process
y0	trav*ss	Beam centroid position in y axis as a function of time
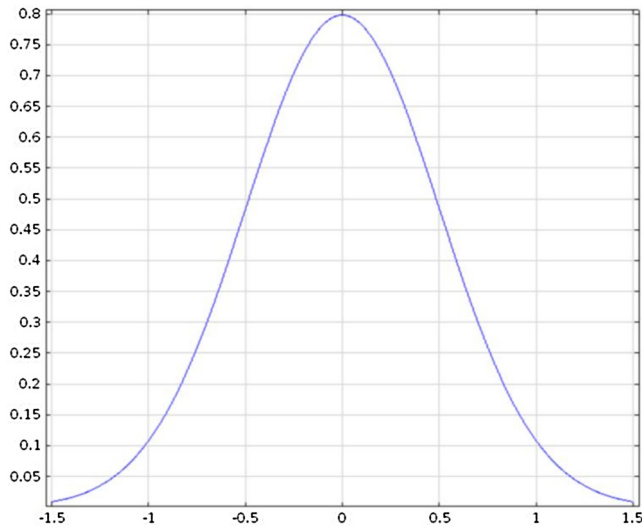
FIG. 5. Plot of Gaussian function.

mean values of n and k of 2.878 and 0.091, respectively. Fresnel relationships, with an assumption of 0° angle of incidence, and these n and k values gave laser absorption values of approximately 76%, which was incorporated into the simulations.

The sides and lower surface of the model were set with insulating boundary conditions, with the upper surface set with both convective and radiative boundaries.

B. Definition of model parameters

In order to aid control of the model, its properties were all defined in a single parameter table, given in Table I.

The position and motion of the beam were controlled by the system of variables given in Table II.

The simulation was designed for a single beam traverse. It was not possible to incorporate repeated oscillating passes at this point in model development.

C. Creation of laser beam heat fluxes

The functions used for this study to model the heat flux from the various beam profiles are described below.

1. Modeling the Gaussian heat flux

In order to model a Gaussian beam, a Gaussian Pulse (gp1) function was created, with a standard deviation of ½. This is shown in Fig. 5.

The variable shown in Table III was created in order to convert the 2D plot into a 3D plot. The use of a standard deviation of ½ in Fig. 5 meant that the heat flux had a $1/e^2$

TABLE III. Gaussian heat flux function.

Variable description	Variable function and name
Applied Gaussian (Q_app)	(P_laser/r_beam^2)*gp1((x-x0)/r_beam)*gp1 ((y-y0)/r_beam) heat flux

TABLE IV. Pedestal heat flux function.

Variable description and name	Variable function
Applied Gaussian heat flux (Q_app_ped)	P_laser/(4*r_beam^2)*if(abs(x-x0) <=r_beam,1,0)*if(abs(y-y0)<=r_beam,1,0)

diameter that matched the r_beam beam radius parameter given in Table I. The laser beam was then specified using the function given in Table III.

Use of this function allowed the Gaussian plot to be controlled using laser beam parameters: the laser power and beam radius. This gave the Gaussian plot shown in Fig. 3(a).

2. Modeling the 3D pedestal laser beam

With the square pedestal beam, the beam design process could be made simpler. In this case, no function plot was necessary and the beam could be specified by a function directly. This is given in Table IV.

Use of this function allowed beam control based on the parameters table in the same way as the Gaussian beam and gave the pedestal plot shown in Fig. 3(b).

3. Modeling the 3D rugby posts beam

A piecewise function (pw2) was used in order to define the rugby posts profile in the x axis. This was created in terms of "b_w" from Table I and is shown in Fig. 6, where the x axis defines the beam width in meters and the y axis is the beam intensity compared to a pedestal beam of the same laser power and dimensions.

This was then incorporated into a useable 3D heat flux with a pair of variables, as shown in Table V.

D. Study and solver settings

The simulation was set up as a time-dependent study with a range of 0 – "period" seconds with intervals of 0.2 s. COMSOL then autoselected the solver configuration, which was
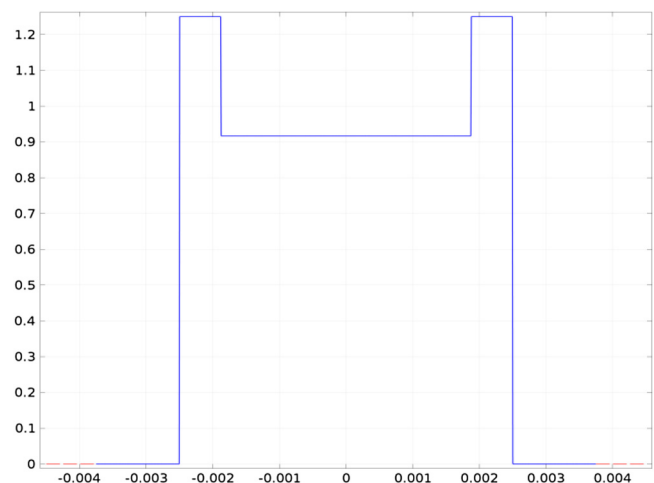
FIG. 6. Plot of Rugby posts function.

TABLE V. Rugby posts heat flux functions.

Variable description and name	Variable function
Conversion of function into variable (F)	pw2(x[1/m])
Applied rugby posts heat flux (Q_app_rug)	(P*F)/((2*a)*(2*b))*if(abs(x-x0)<=a,1,0) *if(abs(y-y0)<=b,1,0)

left as-is. In this case, this was an iterate GMRES solver, rather than a direct MUMPS solver.

Limitations in computing power and workstation availability meant that the period of the simulation was limited to a maximum of 30 s, but it was considered that this did not affect the validity of the results obtained.

IV. SIMULATION RESULTS

This section provides details of the results from heat transfer simulations using the beam profiles described in Sec. III. The results presented here are useful for developing a first approximation of an optimal laser beam profile for annealing.

In this paper, temperature plots have unique color scales reflecting their individual temperature ranges. This method was chosen in order to better visualize the shapes of the temperature profiles in the results. Each plot is shown along with its scale in order to allow temperature comparisons between individual plots.

A. Comparison of a Gaussian laser beam with a square pedestal beam profile

Initial beam shaping involved the altering of the Gaussian profile into a pedestal beam with the same spot dimensions. Figure 7 shows a three-dimensional temperature profile comparison between these two beam types.

The Gaussian beam forms a teardrop shaped temperature profile, based on the circular profile of the beam. When a pedestal beam is applied, the temperature profile becomes squarer and more uniform, following the uniformity of the applied heat flux.

When a pedestal beam is used, the maximum temperature is considerably reduced: from 530 °C to 200 °C. This is the result of two factors. First, because the pedestal beam is square, the beam footprint covers a larger area than the circular Gaussian beam with the same width: $100 \, mm^2$ versus $78.5 \, mm^2$. This reduces the power density applied to the panel and therefore the maximum temperature. Second, the even irradiance profile of the pedestal beam means that there is no concentration of heat in the center, as there is with the Gaussian beam. The temperature at the center of the pedestal beam is therefore not raised to the levels achieved by the Gaussian beam.

This temperature reduction is a side-effect of the greater thermal uniformity afforded by the pedestal beam and can easily be circumvented with an increase in laser power or a reduction in traverse velocity. The benefit lies in the greater thermal uniformity itself.

In contrast to the Gaussian beam, the pedestal beam results in a shallower thermal gradient when heating, and a shorter but steeper cooling gradient. This is shown in Fig. 8, where the temperatures for both beam types (of equal power) are plotted at the top surface along the central line of the beam path.

The leading edge of the pedestal beam begins heating at $15\,500 \, \mu m$ and creates a steep temperature gradient from 20 to 60 °C over a distance of $700 \, \mu m$. There is then a relatively linear increase in temperature until the maximum is reached at $5500 \, \mu m$, at the trailing edge of the beam.

Figure 9 shows a 2D temperature cross-section comparison, each taken at the point of maximum temperature along the y axis, as taken from Fig. 8.

Although the substrate reaches a lower temperature with the pedestal beam compared to the Gaussian beam, as shown in Fig. 8, the temperature occurs uniformly across the majority of the beam's width, whereas the Gaussian beam has the majority of the heating confined to the central

Time = 5 s Isosurface: Temperature (degC) Arrow Volume: Total heat flux
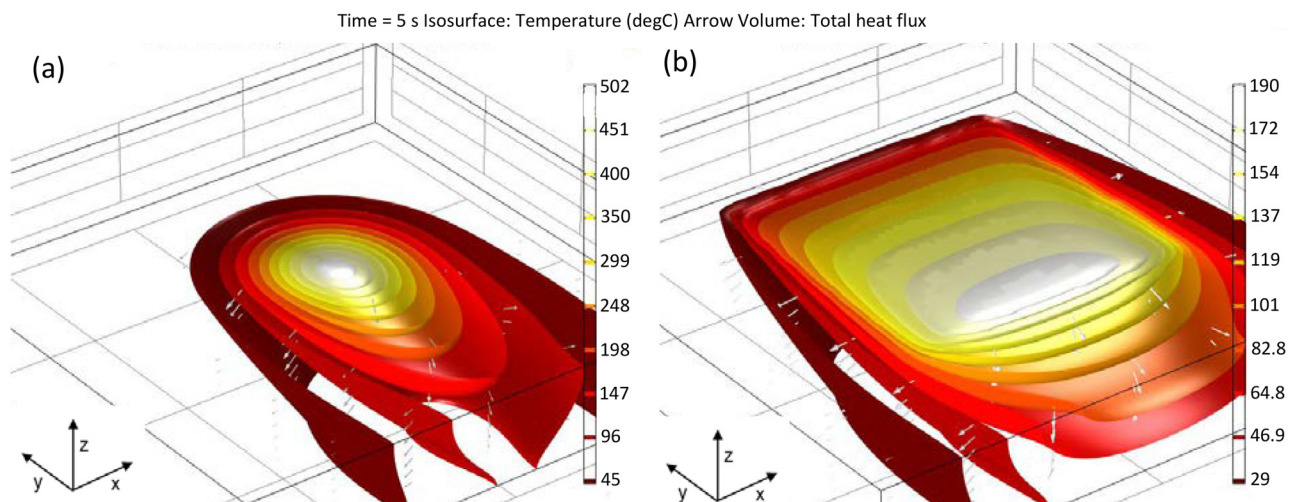
FIG. 7. 3D isothermal contours of (a) 10 mm diameter Gaussian beam and (b) 10 mm pedestal beam.
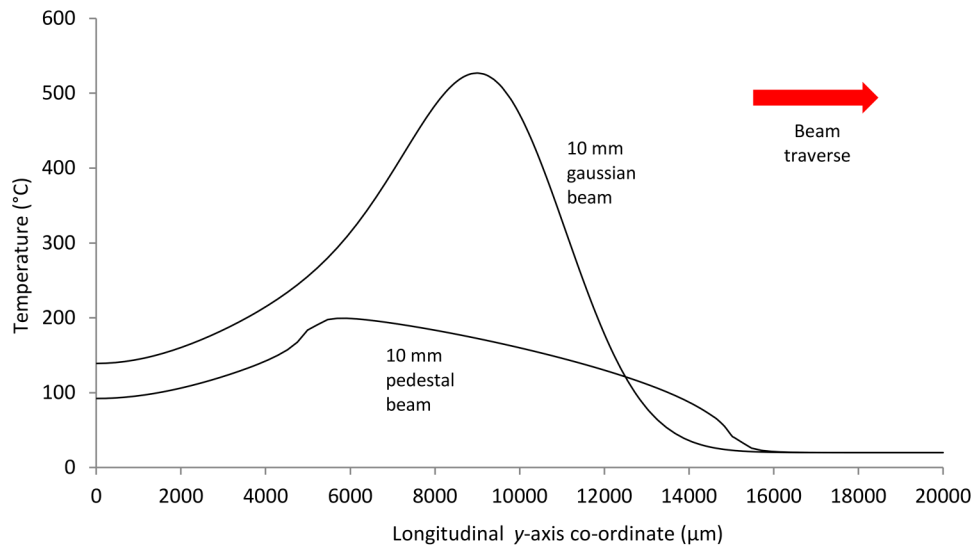
FIG. 8. Longitudinal temperature plots of 10 mm Gaussian vs pedestal beam.

region of the beam, although this area reaches a much higher temperature for a given power. The altered heat-affected zone of the pedestal beam is beneficial in two ways. First, it allows a greater area to be processed for a given traverse rate, which decreases the processing time. Second, the greater level of uniformity in the pedestal beam gives improved consistency for material properties within the panel itself (potentially improving performance and reducing the risk of damage). Use of the Gaussian beam yields alternating bands of highly processed material and underprocessed materials. With the pedestal beam, this effect would be greatly reduced.

B. Comparison of a square pedestal beam profile with a square rugby posts beam profile

In Fig. 10, 3-dimensional plots of the isothermal contours for the pedestal and rugby posts beams are given. The addition of peaks to the outer edges of the laser thermal profile gives further improvements in the homogeneity of the temperature profile in the substrate. In Fig. 10(b), the contours show a greater degree of homogeneity across the beam width, when compared to Fig. 10(a), where there is curvature at the edges.

In Fig. 11, 2D temperature profiles are shown for the two beam types, where the depth of thermal penetration appears to be maintained across a greater portion of the width of the heat-affected zone for the rugby posts beam. Similar to the comparison presented later in Sec. VI, this improved uniformity results in a decrease in maximum temperature.

A numerical analysis of the relative temperature distributions provided by the three beam profiles described is given in Fig. 12. Here, a single isothermal contour is set at 100 °C, placing it near the centers of the temperature scales in Fig. 11, and plotted for all beam types. In order to better show the differences in curvature of the temperature profiles, the plots are stretched in the y axis.

Although the pedestal beam produces greater uniformity in temperature profile compared to a Gaussian beam as
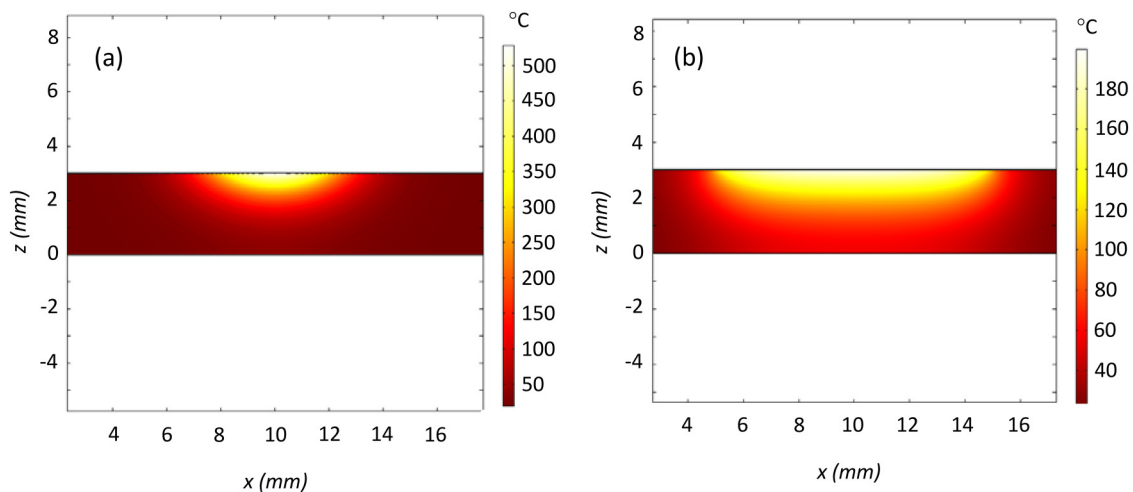
FIG. 9. 2D temperature profiles of (a) 10 mm diameter Gaussian beam and (b) 10×10 mm pedestal beam.

Time = 5 s Isosurface: Temperature (degC) Arrow Volume: Total heat flux
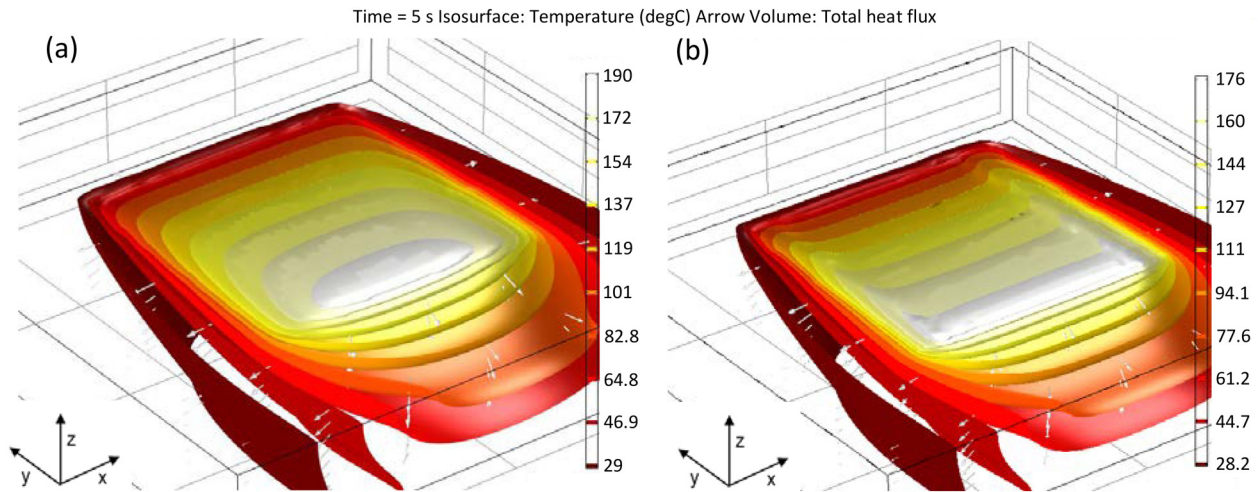
FIG. 10. 3D isothermal contours of (a) 10×10 mm pedestal beam and (b) 10×10 mm rugby posts beam.

shown in Fig. 9, it still produces a curved shape; however, the curve is flat enough so as to give an appearance of uniformity in Fig. 11. When a small amount of additional heat is placed at the edges of the beam, a 4.4 mm wide area of uniformity is introduced (delineated in Fig. 12), equating to 44% of the total beam width. Further beam profile development could be used to reduce the radii of the curvature at each side of the profile.

In a cross-sectional view of heat conduction therefore, the use of a rugby posts beam gives clear advantages in uniformity of temperature compared to pedestal or Gaussian beams. A longitudinal plot is given in Fig. 13, comparing the heating and cooling of the pedestal beam versus the rugby posts beam.

The rugby posts beam results in a lower maximum temperature than in the pedestal beam. This is due to the fact that in order to give a uniform transverse temperature profile, the rugby posts beam relocates energy from the center to the edge of the beam, thereby lowering the energy irradiance in the center and correspondingly the maximum temperature along that line. The two longitudinal temperature profiles

follow the same thermal cycle, since both have a rectilinear irradiance profile in their longitudinal axis.

V. EXPERIMENTAL PROCEDURE

An experimental campaign was undertaken to allow the comparison of the results obtained from computation modeling with physical results obtained within the laboratory. Nominally, 20×20 mm CdTe samples were created on 3 mm thick TEC-10™ glass substrates, with $2 \mu m$ thick CdTe, 100 nm CdS, and 350 nm TCO layers. An example of the samples used is shown in Fig. 14.

A fiber-delivered 808 nm diode laser, mounted on a peltier cooling system, was used to provide the beam and set to 10 W. A fixed-focus collimator was used to form the beam to a 5 mm $1/e^2$ diameter and used for Gaussian experiments. In order to create the holographic beam, a HOE was incorporated into the beam path, which created a 3.5×3.5 mm beam. The intended beam profile was of a slightly modified rugby posts profile with three ramping stages to reduce thermal stresses in the samples. Figure 15 shows a
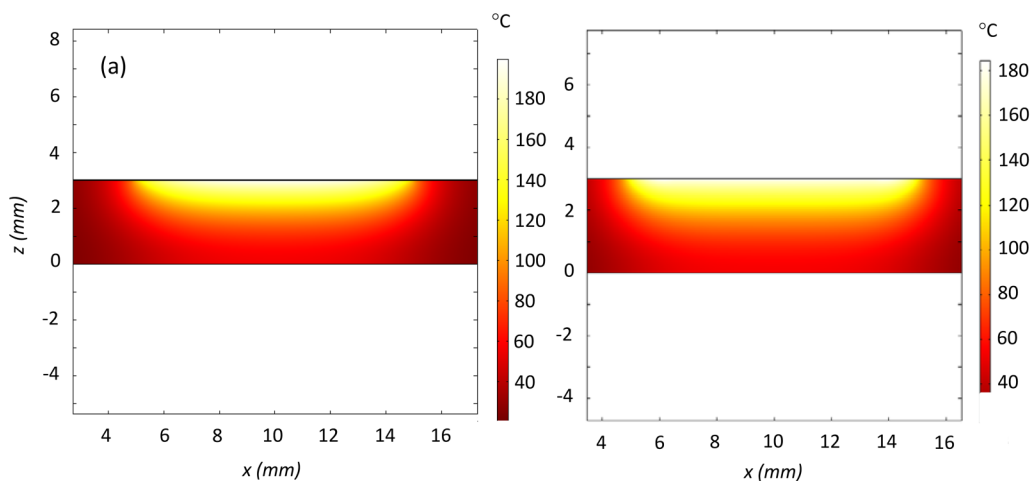
FIG. 11. 2D temperature profiles of (a) 10×10 mm pedestal beam and (b) 10×10 mm rugby posts beam.
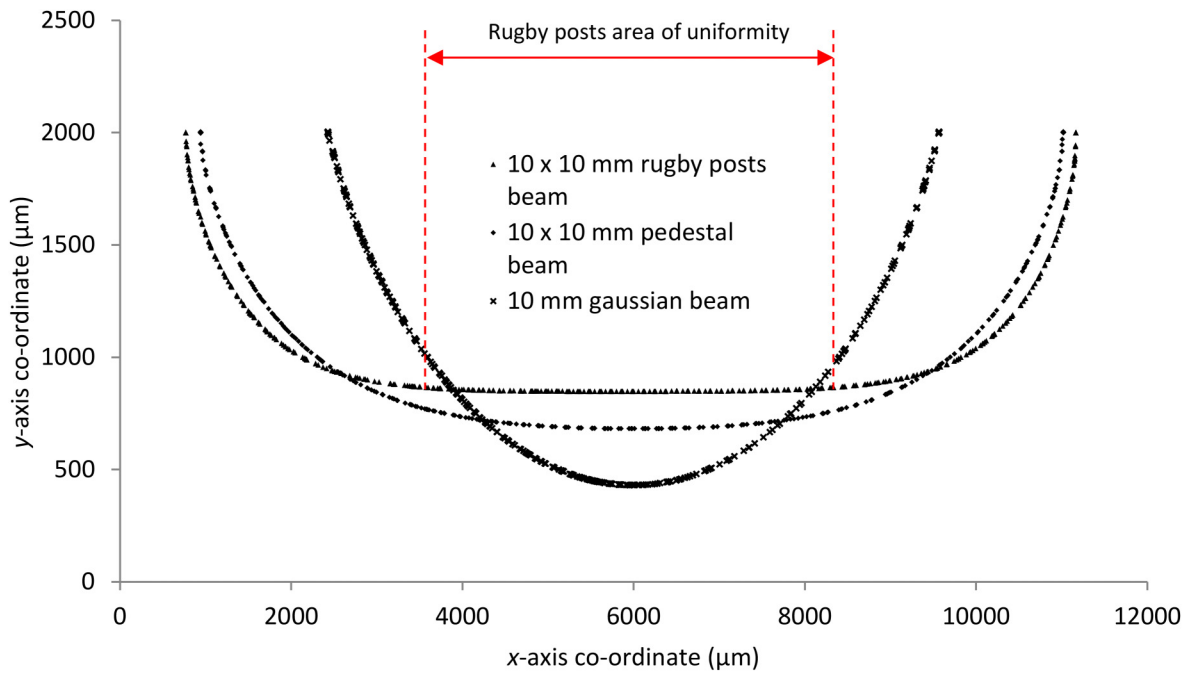
FIG. 12. 2D plots of thermal profiles for 10 mm Gaussian beam, 10 × 10 pedestal beam and 10 × 10 rugby posts beam.

comparison between the proposed energy distribution and the physical output beam created by the HOE.

The HOE demonstrated a reasonable ability to replicate the intended beam profile. A bright center zero-order spot was present in the HOE modified beam, obscuring some of the detail, which was an artifact of the beam energy redistribution. Multiple iterations and refinement of the HOE manufacturing techniques were able to greatly reduce this effect, but it was not completely eliminated.

In the same way as the simulations, the laser beam was oscillated over a 10 mm line at a velocity of 11 mm/s using a 2-axis CNC table. In experimentation, a longer time was possible and the process was continued for several minutes in order to collect more temperature data than was allowed by the computational limitations of the simulation process.

A Flir Thermovision A40 thermal camera using ThermaCam software was used to record the surface temperature during this time. Temperature profile data were then extracted from these recordings for comparison with the simulation results. Multiple results were created for each beam type in order to evaluate repeatability.

VI. EXPERIMENTAL RESULTS

A. Longitudinal temperature distributions

Figure 16 shows the surface temperature along the axis of the Gaussian beam path in the center of the beam, as a counterpart to Fig. 8. The thermal profile closely matches the pattern seen in Fig. 8, with the laser boundaries outlined in
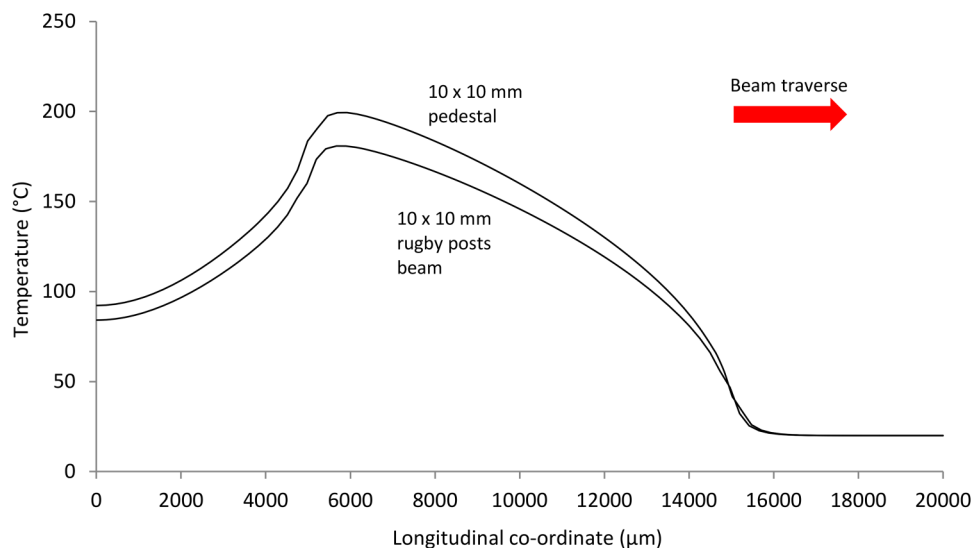
FIG. 13. Longitudinal temperature plots of 10 mm square pedestal beam vs 10 × 10 mm rugby posts beam.
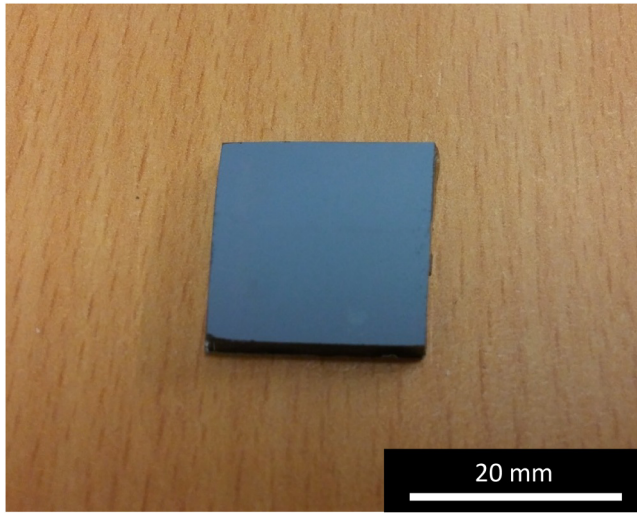
FIG. 14. CdTe sample.

red. Maximum temperatures are considerably lower, 140–200 °C maximum for the experiment versus over 500 °C for the simulation. This means that the Gaussian beam simulation is accurate by comparison to the shape of its temperature distribution, but not in respect to the predicted temperatures. There are a number of potential reasons for this discrepancy:

- Due to the different processing conditions (laser beam traverse speed and beam width)
- Reduced beam power due to absorption/scattering from optics (i.e., HOE)
- Faster than expected conduction of heat for the composite material
- Inaccuracies/interference with the IR thermometry

The similarities in temperature distribution indicate that there is some value in the modeling process to support beam shape design, but further work is required to identify and eliminate the sources of discrepancy for the modeled and observed maximum temperatures.

Figure 17 shows the surface temperature along the axis of the HOE modified beam [shown in Fig. 15(a)] path in the center of the beam, as a counterpart to Fig. 13. It displays subtle differences in temperature distribution between the HOE and Gaussian beams. The same temperature peak is present, with a similar magnitude (140–180 °C) but with a narrower variation in temperatures between individual samples. The HOE-generated temperature profiles also exhibit a sharper temperature peak, which is reflective of the shape of the zero-order hot spot shown in Fig. 15(b). However, because the beam is narrower, the temperature difference within the beam itself between the center and the edge is reduced for the HOE modified beam, from approximately 200–120 °C for the Gaussian, to approximately 180–140 °C.
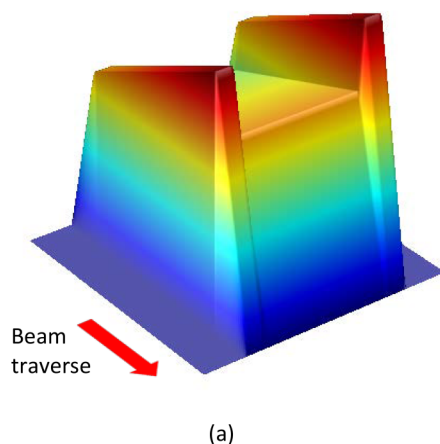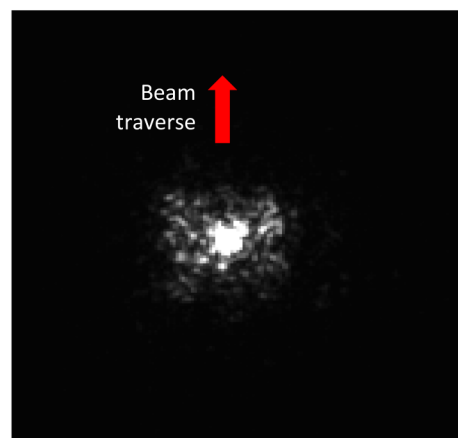
B. Comparison of transverse temperature distributions

The transverse temperature plots both follow a broadly Gaussian pattern. Figure 18 shows transverse temperature plots for the 5 mm Gaussian beam, with the $1/e^2$ boundaries of the beam shown in red.

Figure 19 shows the equivalent plots for the HOE-generated beam, with the beam boundaries outlined in red.

The narrower beam width of the HOE temperature profile results in a sharper peak than the Gaussian beam, where temperature profile more closely follows the beam shape. With the HOE beam and its more even heat profile, high temperatures of approximately 120 °C are maintained at the edge of the beam, compared to a peak of approximately 180 °C, whereas with the Gaussian beam, the edge temperature is reduced to approximately 90 °C from a maximum peak of around 190 °C. Despite the fact that the central hot spot in the HOE seems to have caused a very "Gaussian-like" temperature pattern, the HOE still appears effective in smoothing out the temperature distribution within the laser beam boundaries, by comparison to the Gaussian beam.

C. Sample shattering behavior

An unexpected result that was not predicted in simulation was the shattering of samples. This occurred in around 80% of tested samples in a highly repeatable fashion.

FIG. 15. Images showing (a) 3D computer representation of intended beam geometry and (b) holographically generated laser beam.
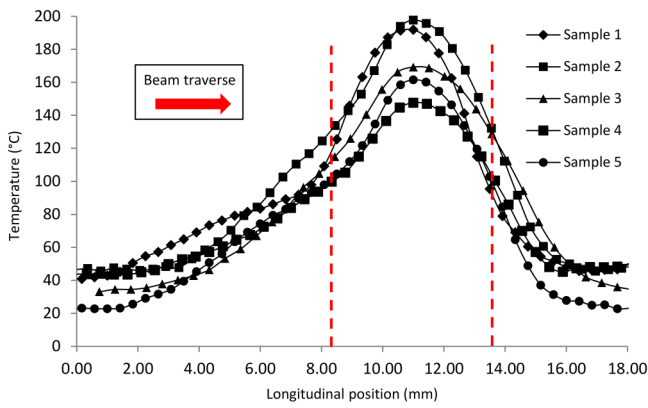
FIG. 16. Longitudinal temperature plots of Gaussian beam.
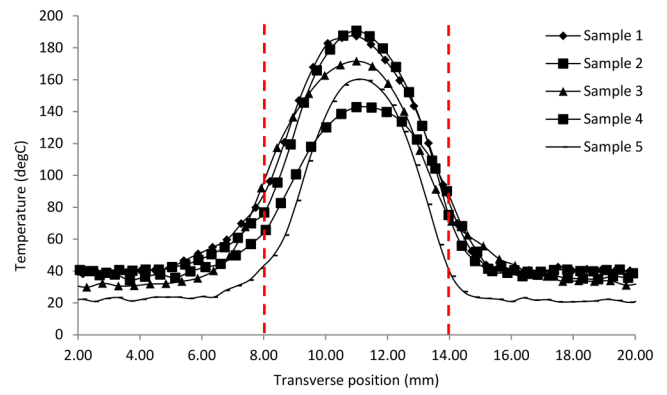
FIG. 18. Transverse temperature plots of Gaussian beam.

Samples were broken in two halves, with the fracture line located at the center of the laser beam path and in the same axis. Figure 20 shows a number of shattered samples, demonstrating the effect and its repeatability.

There appeared to be a dichotomy with sample shattering, where the sample would either not shatter at all or would shatter in this pattern with slight variation depending on the specific sample. If shattering occurred, it always occurred within 2 min of the start of the experiment. If the sample survived this initial period, then it would not shatter during the remainder of the procedure.

It is believed that that the shattering of samples occurred due to the stress being rapidly introduced to the center line of the sample by the laser heating. Due to availability, the size of the samples used in this research were limited to the given dimensions; however, it is predicted that larger samples may not exhibit the same behavior and would survive the rapid heating. The simulation mode did not predict this shatter behavior as it did not consider thermal stresses.

VII. DISCUSSION

An initial review of literature revealed the potential to use lasers as a heat source to anneal CdTe photovoltaics. A laser gives the ability to thermally process only the top-surface semiconductor layer while avoiding the unnecessary bulk heating of the glass substrate. This means that the thermal

processing can be tailored to the panel properties, since laser output can be rapidly adjusted. In addition, laser processing can be halted instantaneously, with no deleterious effects on the panel, an important capability in an age of increasingly unreliable energy supplies. A major limitation identified in existing literature was the need for a galvanometer head to direct the beam at a sufficient velocity to avoid damage to the panel from thermal stresses. Not only does this require a large number of passes to build up a sufficient temperature, it also limits the size of the processing area, since galvanometric heads are limited in how large an area they can cover.

Simulations of thermal heating from a range of incident laser beam profiles were shown to be important for designing appropriate HOE in order to generate the desired thermal profiles in the target material, in this case CdTe. The ability to accurately predict work piece heating allows improved design of HOE without the need for lengthy and costly experimental optimization.

The simulations were found to accurately predict the shape of the temperature profile in the Gaussian beam; however, it was not accurate with regard to predicted temperature levels. This was caused by a number of factors. The difference in temperatures was likely not a function of beam size, since the experimental beam had both a smaller diameter and the lowest temperatures. Likely causes are therefore inaccuracies in the predictions of CdTe heat absorption and heat losses. While the top surface was modeled as convective
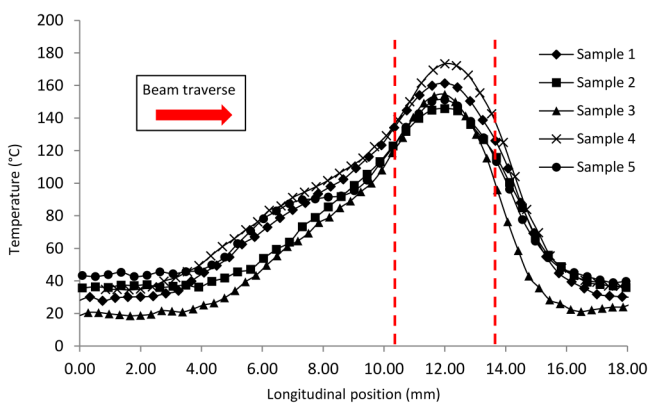
FIG. 17. Longitudinal temperature plots of HOE beam.
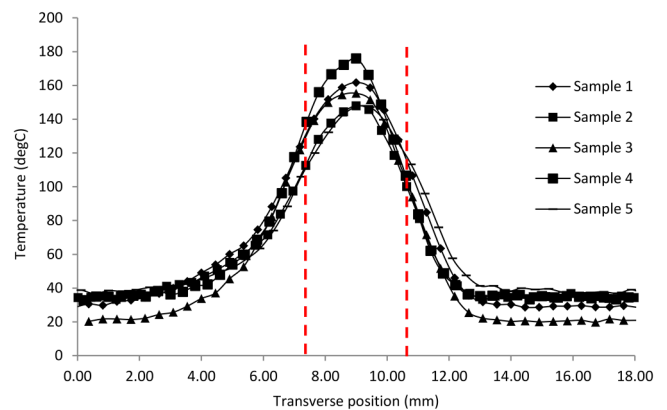
FIG. 19. Transverse temperature plots of HOE beam.
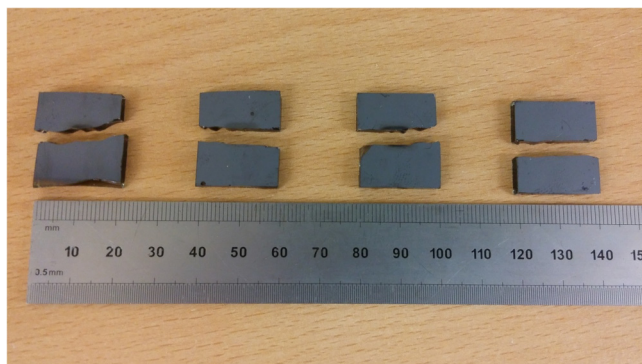
FIG. 20. Image showing shatter pattern of samples.

and radiative, the sides and lower surface were modeled as insulating, whereas in reality they would not provide such thermal isolation. This appears to have resulted in higher levels of heat loss during experimentation than that predicted in the simulations.

With regard to the HOE beam, the HOE was found to be capable of producing reduced thermal gradients within the beam boundaries, compared to the Gaussian beam. However, the HOE-produced temperature profiles bore very little resemblance to the simulated predictions. Some of this would have been due to the same causes as the aforementioned inaccuracies in the Gaussian simulations. The primary cause, however, is due to the presence of the HOE hotspot that could not entirely be eliminated. It is clear from experimental results that this hotspot generated a significant resemblance to a Gaussian beam, from a laser-material interaction point of view. Optical testing of the HOE in Fig. 15 showed that it did form the correct shape, as shown by the reduced thermal gradients in Figs. 17 and 19, but much of the benefit of this was diminished by the presence of the central hotspot.

An unexpected phenomenon not predicted by simulation was the shattering of samples after they were processed for a more extended period of time. The repeatability of this effect, along with the placement of the fracture coincident with the laser beam indicates that this is a result of thermal stresses caused by the laser process. The fact that some samples did not fracture suggests that the thermal stresses, although obviously excessive, were by a relatively small margin. Therefore, only minor adjustments might be necessary, such as an increase in laser beam size in order to spread the thermal stress over a larger area. Further study of this is necessary in order for development of the laser process to proceed. COMSOL does include the ability to model thermal stresses, so future simulation development should allow for sample shattering to be predicted in simulation and thus more easily controlled.

VIII. CONCLUSIONS

The following conclusions can be drawn from this work:

- HOEs can be used to generate a physical laser beam that matches a unique simulated temperature profile at 808 nm. The beam is an accurate recreation with further development required to remove the observed hotspot.

- COMSOL can be used to create simulations of customized nonlinear laser beam thermal profiles, allowing models to be created to optimize laser beam heat flow in materials processing applications.
- The use of HOEs was successful in creating more uniform surface temperatures within the laser beam boundaries, compared to a Gaussian beam. The presence of a hotspot in the HOE reduces the uniformity compared to simulated predictions however.
- Refinements of the model and of the experimental setup are required to better match the predicted and observed temperature ranges of the sample during processing.
- Further simulation development is required in order to better account for heat absorption, heat loss and thermal stresses within the model.
- The scalability of the HOE laser annealing approach lends itself to industrial application. With the use of an accurate model, such a technology is viable for main stream manufacturing of thin-film photovoltaics.

[1]Department for Energy and Climate Change, *UK Solar PV Strategy Part 1: Roadmap to a Brighter Future* (Department for Energy and Climate Change, London, 2013).

[2]Department for Energy and Climate Change, *Digest of the United Kingdom Energy Statistics (DUKES)* (Department for Energy and Climate Change, London, 2015).

[3]S. Kann, M. Shiao, S. Mehta, C. Honeyman, N. Litvak, J. Jones, J. Baca, W. Lent, and S. Rumery, *U. S. Solar Market Insight Report | 2014 Year in Review | Executive Summary* (Washington: Solar Energy Industries Association, Washington, 2014).

[4]J. Poortmans and V. Arkhipov, *Thin Film Solar Cells* (John Wiley & Sons Ltd., Chichester, 2006).

[5]J. Peng, L. Lu, and H. Yang, "Review on life cycle assessment of energy payback and greenhouse gas emission of solar photovoltaic systems," Renew. Sustain. Energy Rev. **19**, 255–274 (2013).

[6]M. J. De Wild-Scholten, "Energy payback time and carbon footprint of commercial photovoltaic systems," Sol. Energy Mater. Sol. Cells **119**, 296–305 (2013).

[7]J. D. Major, R. E. Treharne, L. J. Phillips, and K. Durose, "A low-cost non-toxic post-growth activation step for CdTe solar cells," Nature **511**, 334–337 (2014).

[8]M. D. G. Potter, D. P. Halliday, and M. A. Cousins, "Analysis of CdCl2 annealing process in CdTe/CdS solar cells," in 16th European Photovoltaic Solar Energy Conference (2000), Vol. 16, pp. 847–850.

[9]N. Spalatu, J. Hiie, V. Valdna, M. Caraman, N. Maticiuc, V. Mikli, T. Potlog, M. Krunks, and V. Lughi, "Properties of the CdCl₂ air-annealed CSS CdTe thin films," Energy Procedia **44**, 85–95 (2014).

[10]A. Abbas, G. D. West, J. W. Bowers, P. Isherwood, P. M. Kaminski, B. Maniscalco, P. Rowley, J. M. Walls, K. Barricklow, W. S. Sampath, and K. L. Barth, "The effect of cadmium chloride treatment on close-spaced sublimated cadmium telluride thin-film solar cells," IEEE J. Photovolt. **3**, 1361–1366 (2013).

[11]D. Triantafyllidis, J. R. Bernstein, L. Li, and F. H. Stott, "Dual laser beam modification of high alumina ceramics," J. Laser Appl. **15**, 49–54 (2003).

[12]A. F. H. Kaplan, "Surface processing with non-Gaussian beams," Appl. Phys. Lett. **70**, 264–266 (1997).

[13]D. Lee and J. Mazumder, "Effects of laser beam spatial distribution on laser-material interaction," J. Laser Appl. **28**, 032003 (2016).

[14]B. J. Simonds, H. J. Meadows, S. Misra, C. Ferekides, P. J. Dale, and M. A. Scarpulla, "Laser processing for thin film chalcogenide photovoltaics: a review and prospectus," J. Photonics Energy **5**, 050999 (2015).

[15]N.-H. Kim, C. Il Park, and H.-Y. Lee, "Microstructure, stress and optical properties of CdTe thin films laser-annealed by using an 808-nm diode laser: Effect of the laser scanning velocity," J. Korean Phys. Soc. **63**, 229–235 (2013).

[16]N.-H. Kim, C. Il Park, and J. Park, "A pilot investigation on laser annealing for thin-film solar cells: Crystallinity and optical properties of laser-annealed CdTe thin films by using an 808-nm diode laser," J. Korean Phys. Soc. **62**, 502–507 (2013).

[17]B. J. Simonds, S. Misra, N. Paudel, K. Vandewal, A. Salleo, S. Feredikes, and M. A. Scarpulla, "Near infrared laser annealing of CdTe and in-situ measurement of the evolution of structural and optical properties," J. Appl. Phys. **119**, 165305 (2016).

[18]W. W. Duley, *Laser Welding* (John Wiley & Sons Ltd., New York, 1999).

[19]V. Weerasinghe, J. Gabzdyl, and R. Hibberd, "Properties of a laser beam generated from an axicon resonator," Opt. Laser Technol. **21**, 389–391 (1989).

[20]D. Wellburn, S. Shang, S. Wang, Y. Sun, J. Cheng, J. Liang, and C. S. Liu, "Variable beam intensity profile shaping for layer uniformity control in laser hardening applications," Int. J. Heat Mass Transf. **79**, 189–200 (2014).

[21]S. H. Mok, G. Bi, J. Folkes, and I. Pashby, "Deposition of Ti–6Al–4V using a high power diode laser and wire, Part I: Investigation on the process characteristics," Surf. Coat. Technol. **202**, 3933–3939 (2008).

[22]A. Riveiro, A. Mejías, F. Lusquiños, J. del Val, R. Comesaña, J. Pardo, and J. Pou, "Laser cladding of aluminium on AISI 304 stainless steel with high-power diode lasers," Surf. Coat. Technol. **253**, 214–220 (2014).

[23]J. Tyrer and S. Noden, "Diffractive optical elements for manipulation of high power CO2 laser radiation – a feasibility study," in High-Power Lasers: Applications and Emerging Applications (SPIE, Washington, 1996), Vol. 2789.

[24]R. Higginson, M. Gibson, J. Kell, and J. Tyrer, "Weld pool shaping and microstructural control using novel computer generated holographic optic laser welding of steel and stainless steel," Mater. Sci. Forum **638–642**, 3673–3678 (2010).

[25]J. Kell, J. Tyrer, R. Higginson, J. Jones, and S. Noden, "Laser weld pool management through diffractive holographic optics," Mater. Sci. Technol. **28**, 354–363 (2011).

[26]R. Higginson, M. Blackmur, M. Gibson, and J. Tyrer, "Grain size control in the weld pool and heat affected zone using holograms," Mater. Sci. Forum **715–716**, 340–345 (2012).

[27]N. J. Goffin, S. Hou, J. R. Tyrer, and R. L. Higginson, "The use of holographic optics for heat flow control in wire-based laser cladding," in Proceedings of the 33rd International Congress on Applications of Lasers and Electro-Optics 2014 (Laser Institute of America, Orlando, 2014), pp. 383–392.

[28]N. Goffin, R. Higginson, and J. Tyrer, "The use of Holographic Optical Elements (HOE's) to investigate the use of a flat irradiance profile in the control of heat absorption in wire-fed laser cladding," J. Mater. Process. Technol. **220**, 119–201 (2015).

[29]F. Lisco, N. Goffin, A. Abbas, G. Claudio, E. Woolley, J. Tyrer, and J. Walls, in 43rd IEEE Photovoltaics Specialists Conference, Portland, OR, 5–10 June 2016.

[30]E. Palik, *Handbook of Optical Constants of Solids* (Harcourt Brace Jovanovich, Boston, 1985).

Meet the Authors

Nicholas Goffin has a PhD in the field of holographic optics for use in laser assisted cladding from Loughborough University. In 2015 he became a Postdoctoral Researcher working on laser annealing of thin-film photovoltaics, also at Loughborough University. He is currently a Research Engineer at the Manufacturing Technology Centre in Coventry, UK.

John Tyrer is a member of the Optical Engineering Research Group at Loughborough University where he has worked for over two decades. A Mechanical Engineer by education, John is a laser materials processing expert who has pioneered the use of computer generated holographic optics for custom beam generation to improve material properties of laser processed parts. The author of over 200 journal and conference papers, he has chaired a number of Laser Institute of America (LIA) Conferences, for which he is on the board of directors, and a Fellow.

Elliot Woolley is a Lecturer in Sustainable Manufacturing in the Centre for Sustainable Manufacturing and Recycling Technologies at Loughborough University. With an educational background in the field of Applied Physics, his PhD research developed high power laser devices for optical pumping of gases with applications in material spectroscopy. Elliot's current research focus is on the understanding and rationalization of energy consumption within manufacturing plants and processes and in the development of novel approaches to realize radical energy efficiency improvements. Elliot was principle investigator for the EPSRC funded project EP/M014088/1.